A Comprehensive Line Spread Function Error Budget for the Off-Plane Grating Rocket Experiment

Benjamin D. Donovan[a], Randall L. McEntaffer[a], James H. Tutt[a], Bridget C. O'Meara[a], Fabien Grisé[a], Kim A. Allgood[b,c], Michael P. Biskach[b,c], Kai-Wing Chan[b,d], Michal Hlinka[b,c], John D. Kearney[b,c], James R. Mazzarella[b,c], Ryan S. McClelland[b,c], Ai Numata[b,c], Raul E. Riveros[b,d], Timo T. Saha[b], Peter M. Solly[b,c], William W. Zhang[b], Andrew D. Holland[e], Matthew R. Lewis[e], Matthew R. Soman[e], and Karen Holland[f]

[a]The Pennsylvania State University, University Park, PA 16802
[b]NASA Goddard Space Flight Center, Greenbelt, MD 20771
[c]KBRwyle Space Engineering Division, Greenbelt, MD 20770
[d]University of Maryland-Baltimore County, Baltimore, MD 21250
[e]The Open University, Walton Hall, Milton Keynes, UK
[f]XCAM Ltd., Northampton, UK

ABSTRACT

The Off-plane Grating Rocket Experiment (OGRE) is a soft X-ray grating spectrometer to be flown on a suborbital rocket. The payload is designed to obtain the highest-resolution soft X-ray spectrum of Capella to date with a resolution goal of $R(\lambda/\Delta\lambda) > 2000$ at select wavelengths in its $10 - 55$ Å bandpass of interest. The optical design of the spectrometer realizes a maximum resolution of $R \approx 5000$ with all components performing optimally, in perfect alignment, and not considering in-flight pointing errors; however, performance errors, misalignments, and in-flight pointing errors work to degrade this performance. A comprehensive line spread function (LSF) error budget has been constructed for the spectrometer to identify errors contributing to the LSF, to determine how each affects the LSF, and to inform performance requirements and alignment tolerances for the spectrometer. In this document, the comprehensive LSF error budget for the OGRE spectrometer is presented and its implications are discussed.

Keywords: error budget, alignment tolerances, performance requirements, soft X-ray spectroscopy, reflection gratings, mono-crystalline silicon X-ray optics, electron-multiplying CCDs

1. INTRODUCTION

The Off-plane Grating Rocket Experiment (OGRE) is a soft X-ray grating spectrometer that will be flown on a suborbital rocket. With a spectral resolution requirement of $R(\lambda/\Delta\lambda) > 1500$ across its $10 - 55$ Å bandpass of interest and a spectral resolution goal of $R > 2000$ at select energies in this bandpass, OGRE will obtain the highest-resolution soft X-ray astronomical spectrum to date. This performance will enable OGRE to examine the soft X-ray spectrum of its target, Capella (α Auriga), in unprecedented detail. This detailed observation will permit existing line blends in the soft X-ray spectrum of Capella to be resolved, new and updated emission lines to be integrated into plasma spectral models, and more accurate plasma characteristics to be determined for this source.[1]

To attain the performance goal of $R > 2000$, OGRE will employ cutting-edge technologies for each of its three spectrometer components: a mono-crystalline silicon X-ray optic module manufactured by NASA Goddard Space Flight Center,[2] six reflection grating modules developed by The Pennsylvania State University operated in the extreme off-plane mount,[3] and an array of four electron-multiplying CCDs (EM-CCDs) manufactured by e2v and integrated into a camera package by XCAM Ltd. and The Open University.[4]

In the extreme off-plane mount, light is incident at grazing incidence and quasi-parallel to the groove direction as depicted in Figure 1. Diffraction then follows the generalized grating equation:
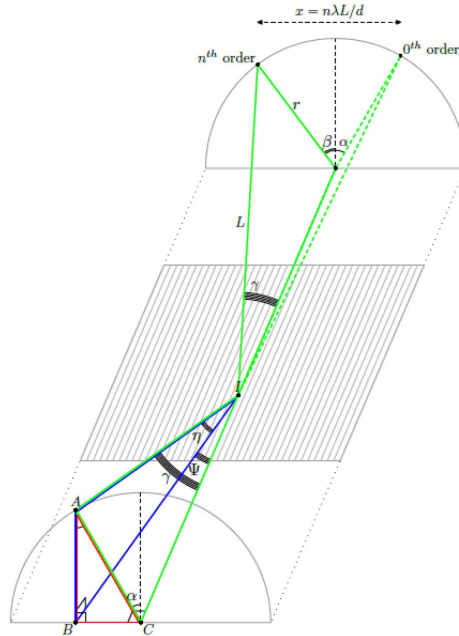

Figure 1: The diffraction geometry of a reflection grating in the extreme off-plane mount.[5] (a): Light is incident from point A onto the grating surface at a graze angle η and relative to the groove direction by an angle Ψ. Equivalently, this incidence geometry can be described in the spherical coordinate system by azimuth angle α and polar angle γ. Diffraction follows the generalized grating equation (Eq. 1) and light is diffracted a distance L to azimuth angle β on the focal plane. The dispersion distance between the $n = 0$ reflection and n-th diffraction order on this focal plane is given by $x = n\lambda L/d$.

$$\sin\alpha + \sin\beta = \frac{n\lambda}{d\sin\gamma}, \tag{1}$$

where α is the incident azimuthal angle, β is the diffracted azimuthal angle, γ is the polar angle between the incident light and the groove direction, d is the groove period, n is the diffraction order, and λ is the wavelength of the light.[6] By differentiating Eq. 1 with respect to λ, it can be shown that:

$$\frac{d\lambda}{dx} = \frac{10^7}{nLD}\frac{\text{Å}}{\text{mm}}, \tag{2}$$

where L is the distance a photon on the grating travels to the spectrometer focal plane, D is the groove density ($\equiv 1/d$), and x is the distance a photon is diffracted from the $n = 0$ reflection ($= L\sin\gamma(\sin\beta + \sin\alpha)$). This equation shows that while the extreme off-plane mount diffracts its incident light conically, the spectral information is contained only in one dimension – the dispersion direction (x in Figure 1).

The OGRE optic module is divided into six 60° azimuthal segments. Behind each of these azimuthal segments is a grating module containing 60 individual gratings organized into two side-by-side grating stacks. The grating positions in each module are numerically optimized to realize maximum spectral resolution at the Fe XVII emission line ($\lambda = 15.01$ Å) – the brightest line expected to be observed by OGRE from Capella. Light from two neighboring grating modules is then diffracted to the same location on the focal plane where the spectra are read out by a single detector. A schematic of this geometry can be seen in Figure 2. A further discussion of this diffraction geometry can be found in Donovan et al. (2019).[1]

The optical design of the OGRE spectrometer realizes a maximum spectral resolution of $R \approx 5000$. However, this resolution is only attained if all spectrometer components perform flawlessly, if these components are all
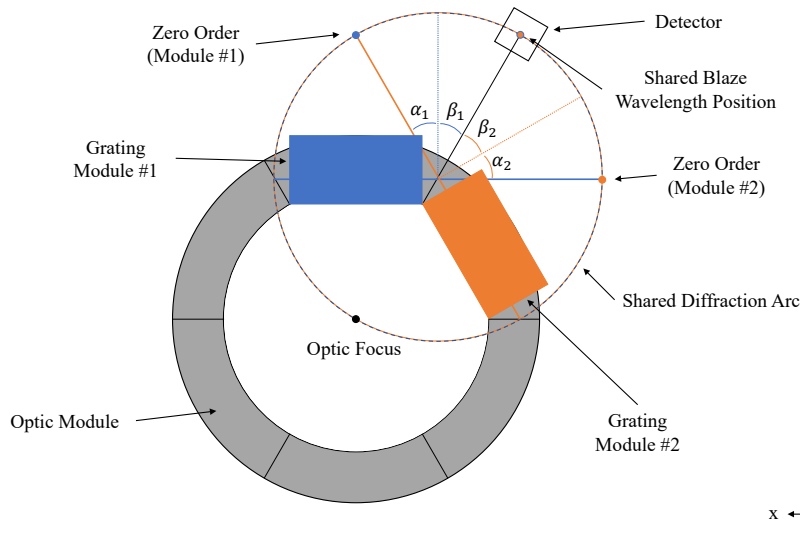
Figure 2: Diffraction geometry for neighboring grating modules in the OGRE soft X-ray spectrometer.[1] The optic module is divided into six 60° azimuthal segments. Behind each of these segments is a grating module containing 60 gratings. To maximize diffraction efficiency, each grating module operates in the Littrow mount which requires $\alpha = \beta = \delta$. For the OGRE spectrometer, $\alpha = \beta = \delta = 30°$ such that the neighboring grating modules diffract to the same location on the focal plane. This geometry is repeated two times to populate the entire 360° azimuthal span of optic with grating modules. Depicted in the bottom-right is the coordinate system for this schematic view.

perfectly aligned, and if the payload remains oriented exactly towards its target. However, each component in the spectrometer in reality does not perform at this level and the payload does not remain oriented in this manner. The measured performance of the gratings in the OGRE grating modules and the mirror segments in the OGRE optic module will deviate from their theoretical performance. These performance errors will begin to degrade the observed line spread function (LSF) of the spectrometer. Furthermore, the spectrometer components will not be placed perfectly with respect to each other. These misalignments will decrease the performance of the spectrometer further. Finally, the spectrometer will not remain perfectly pointed at Capella during its observation, but will jitter about the ideal pointing. This in-flight jitter will further degrade the observed LSF. Therefore, the the spectrometer will not achieve its theoretical spectral resolution of $R \approx 5000$, but will achieve a performance below this level.

To understand how each misalignment and error contributes to the performance of the OGRE spectrometer, a comprehensive LSF error budget is required. This error budget identifies each contribution to the LSF, determines how each of these contributions affects the observed LSF, and then ultimately informs performance requirements and alignment tolerances for the OGRE spectrometer. In this manuscript, the comprehensive LSF error budget for OGRE is described and implications resulting from this error budget are discussed.

2. THE COMPREHENSIVE LSF ERROR BUDGET

The comprehensive LSF error budget for OGRE considers potential misalignments and performance errors in the spectrometer. These misalignments and performance errors come from each of the three main components of the spectrometer: the OGRE optic module, the OGRE grating modules, and the OGRE detector array. Additional errors arise from in-flight pointing errors. Each of these misalignments and errors alters the LSF from the idealized LSF of the spectrometer by increasing the extent of the LSF in the dispersion and/or cross-dispersion direction. This behavior directly impacts the achievable spectral resolution and/or the effective area of the spectrometer. Additionally, misalignments can shift the LSF centroid on the detector. These shifts can move important spectral lines of Capella off of the detector, further impacting the achievable performance of the
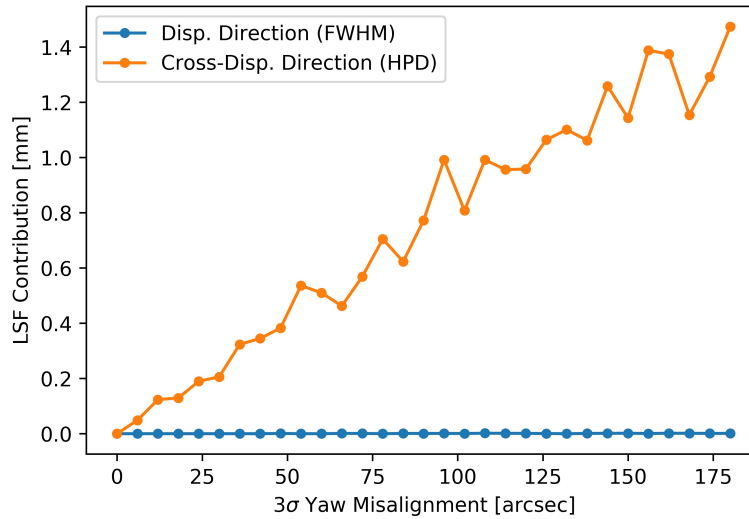
Figure 3: Results from a raytrace simulation of the OGRE spectrometer showing the effect of a yaw misalignment of individual gratings in the grating module on the extent of the OGRE LSF in the dispersion (blue) and cross-dispersion (orange) directions. The contribution in the dispersion direction is measured as a full-width at half-maximum (FWHM), while the contribution in the cross-dispersion direction is measured as a half-power diameter (HPD). Here, it can been seen that a grating-level yaw misalignment at these simulated misalignment values does not contribute to the LSF extent in the dispersion direction, but it has a large impact on the LSF extent in the cross-dispersion direction.

spectrometer. Thus, each potential misalignment and error must be analyzed to ensure performance requirements are met.

The construction of the LSF error budget begins with the consideration of a single error or misalignment. For example, consider the alignment of the 60 individual gratings that comprise a single OGRE grating module. Each grating can be misaligned relative to its nominal placement in all six degrees of freedom: $\hat{x}$, $\hat{y}$, $\hat{z}$, pitch (rotation about $\hat{x}$), yaw (rotation about $\hat{y}$), and roll (rotation about $\hat{z}$). Custom raytrace software is utilized to simulate misalignments in each of these degrees of freedom. An example plot showing how yaw misalignments of the 60 gratings in an OGRE grating module affect the observed LSF at the OGRE spectrometer focal plane is shown in Figure 3. Additional simulations for this misalignment would be obtained for the remaining five degrees of freedom. Then, further simulations are performed to determine the impact of all remaining misalignments and errors on the LSF. Once all simulations have been performed, alignment tolerances and performance errors are assigned after also considering manufacturing limitations, alignment capabilities, performance limits, and other similar inputs. Throughout the construction of this error budget, the performance requirements and/or goals are continually referenced to ensure that the spectrometer will meet these requirements and/or goals. For OGRE, the spectral resolution goal is $R > 2000$ (resolution requirement: $R > 1500$) and the LSF extent in the cross-dispersion direction must remain within the planned window size of the spectral detector (~ 6 mm). While the LSF must remain within this window, movement of the LSF centroid in the cross-dispersion direction can be larger than this since the window can be moved on the detector. Movement must be limited though, as the LSF must still remain on the detector (~ 25 mm x 25 mm).

In the following subsections, individual contributions to the OGRE LSF error budget will be discussed. The discussion here is limited to a single 60° azimuthal segment of the OGRE optic module, a single OGRE grating module placed behind this optic segment, and a single spectral detector. These three components form a single OGRE spectrometer "channel". While this analysis is limited to a single channel, each channel is identical or mirrored with respect to the modeled channel, so the described analysis will apply to the remaining five spectrometer channels as well. Furthermore, this analysis is limited to the wavelength dispersing to the center of a spectral detector: $n\lambda = 4.76$ nm ($x = 98.2$ mm of dispersion).

Table 1: Errors induced to the LSF of the OGRE spectrometer from a 60° azimuthal segment of the OGRE optic module. Since the optic will be treated as an assembled unit, the only errors to consider are its performance in both the dispersion direction (measured as a full-width at half-maximum; FWHM) and the cross-dispersion direction (measured as a half-power diameter; HPD).

| | | Requirements (3σ Level) | | LSF Impact | |
| | | | | Dispersion Direction | Cross-Disp. Direction |
Error	DoF	μm (±)	arcsec (±)	FWHM [μm]	HPD [μm]
PSF (dispersion dir.)			*1.5*	25.4	
PSF (cross-dispersion dir.)			*5.0*		84.8
RSS Total				25.4	84.8

2.1 Optic Contributions

The development of the OGRE optic module is led by NASA Goddard Space Flight Center.[2] The optic module is composed of 288 individual mirror segments: 144 segments form the 12 primary (paraboloid) mirror shells and the remaining 144 segments for the 12 secondary (hyperboloid) mirror shells. Once assembled, it will be delivered to The Pennsylvania State University where it will be integrated into the spectrometer. Since this component is manufactured externally, a detailed error analysis of this component is beyond the scope of this error budget; however, similar error budgets for mono-crystalline optic modules have been developed for other X-ray missions.[7] The presented error budget only considers the final performance of the OGRE optic module in the dispersion and cross-dispersion directions.

The performance requirements of the OGRE optic module are derived from current performance of mono-crystalline optic segments. These segments routinely achieve a point spread function (PSF) with half-power diameter (HPD) of < 5 arcsec.[2] Furthermore, a 60° azimuthal segment is expected to perform at < 1.5 arcsec full-width at half-maximum (FWHM) in the dispersion direction. Thus, these numbers have been adopted as the OGRE optic performance requirements for a single 60° azimuthal segment: < 1.5 arcsec FWHM in the dispersion direction and < 5 arcsec HPD in the cross-dispersion direction. At a focal length of $Z_0 = 3500$ mm, these dispersion and cross-dispersion requirements correspond to < 25.4 μm FWHM and < 84.8 μm HPD, respectively. These errors are summarized in Table 1.

The finite optic performance is the first error impacting the LSF of the OGRE spectrometer. If the only contribution to the LSF is the PSF from this optic, the spectrometer will exactly reproduce the PSF at dispersion. With the spectral detector centered in the dispersion direction at $x = 98.2$ mm, this equates to an achievable spectral resolution of $R(x/\Delta x) \approx 3860$. Therefore, the performance of the OGRE spectrometer has already degraded due to the finite optic performance. However, there are many additional contributions to the LSF that must be considered.

2.2 Grating Contributions

In a grating spectrometer, a large portion of the errors seen in the observed LSF come from the diffractive element in the spectrometer: the gratings. For OGRE, these errors arise from five main sources: aberrations induced by the diffraction geometry, the finite performance of the individual gratings, and three misalignments during the construction of the grating module and the alignment of this grating module to a 60° azimuthal segment of the OGRE optic module. Each of these five error sources will be discussed in the following subsections.

2.2.1 Diffraction Geometry Aberration

The first LSF error from the gratings in the spectrometer comes from the diffraction geometry itself. While the goal of a reflection grating spectrometer such as OGRE is to exactly reproduce the PSF from the optic at dispersion to achieve maximum spectral resolution, this rarely happens in practice. Aberrations are induced which causes the diffracted LSF to diverge from this PSF. For OGRE, the grating positions were numerically optimized to minimize these induced aberrations in the dispersion direction at Fe XVII ($\lambda = 15.01$ Å). As a result of this optimization, the induced LSF aberrations in the dispersion direction were effectively eliminated. However, because this optimization only sought to minimize the aberrations in the dispersion direction, the

Table 2: Grating-induced errors to the observed LSF of the OGRE spectrometer, including aberrations induced by the diffraction geometry itself, the finite resolution limit of the individual gratings, grating-level alignment, stack-level alignment, and module-to-optic alignment. Shown are the 3σ level (99.7%) requirements for each error in all six degrees of freedom (DoF; if applicable) and the impact of the error in both the dispersion direction (measured as a full-width at half maximum [FWHM]) and the cross-dispersion direction (measured as a half-power diameter [HPD]).

Error	DoF	Requirements (3σ Level) μm (±)		arcsec (±)		LSF Impact — Dispersion Direction FWHM [μm]		Cross-Disp. Direction HPD [μm]	
Diffraction Geometry Aberration								60.5	
Finite Grating Resolution Limit				R = 4500		21.8			
Grating-Level Alignment Within Stack	X	127				0.4		102.6	
	Y	127				0.8		0.0	
	Z	127				8.5		0.0	
	Pitch (X)			30		0.0		489.9	
	Yaw (Y)			30		0.6		282.2	
	Roll (Z)			15		10.8		5.7	
Stack-Level Alignment Within Module	X	-127	127			1.0	1.0	179.4	50.9
	Y	-254	254			0.0	0.0	551.9	436.4
	Z	-127	127			3.6	6.7	0.0	21.4
	Pitch (X)			-60	60	0.3	0.0	1910.8	1805.7
	Yaw (Y)			-60	60	3.6	0.0	1019.1	1130.7
	Roll (Z)			-30	30	31.0	26.9	62.6	0.0
Module-To-Optic Alignment	X	-500	500			0.7	1.0	10.4	0.0
	Y	-500	500			0.0	2.0	10.9	0.0
	Z	-1000	1000			1.7	0.0	0.0	39.9
	Pitch (X)			-60	60	1.0	0.0	9.2	0.0
	Yaw (Y)			-60	60	2.1	1.0	0.0	13.8
	Roll (Z)			-120	120	0.0	1.6	4.7	4.1
RSS Total						40.8	38.0	2316.2	2251.2

extent of the LSF in the cross-dispersion direction grew slightly – the LSF error in the cross-dispersion direction due to aberrations induced by the diffraction geometry was 60.5 μm HPD. A summary of this induced LSF error is shown in Table 2.

2.2.2 Grating Performance

The second error in the LSF induced by the gratings in the spectrometer is the aberration due to the finite resolution of the individual gratings. The OGRE spectrometer is designed to utilize gratings with a radial groove profile and a groove period of 160 nm at a distance of 3300 mm from the hub of the converging grooves. However, the processes used to manufacture these gratings cannot perfectly achieve this ideal groove profile. Thus, the manufactured groove profile will deviate slightly from this ideal groove profile.

The manufactured groove profile is expected to deviate from the theoretical groove profile in a Gaussian manner. Therefore, the groove period at any given location on a grating will have a Gaussian distribution about its nominal value. From Eq. 2, this Gaussian groove period error will manifest on the focal plane as a Gaussian error in the dispersion direction. This will then impart an aberration into the observed LSF in this direction. These Gaussian period errors do not impact the cross-dispersion extent. This error is listed in Table 2 as the "Finite Grating Resolution Limit".

OGRE grating prototypes have been tested for spectral resolution at the Max Planck Institute for Extraterrestrial Physics' PANTER X-ray Test Facility in the summer of 2018. Preliminary results from this testing show that an OGRE grating prototype achieved a grating-induced spectral resolution of $R > 4600$ (97.5% confidence level); final results from this testing are forthcoming.[8] Therefore, the requirement for the grating-induced resolution in the LSF error budget has been adopted as $R > 4500$ (3σ). If each grating performs at this level, the impact on the observed LSF in the dispersion direction is 21.8 μm FWHM. This error can be seen in Table 2.
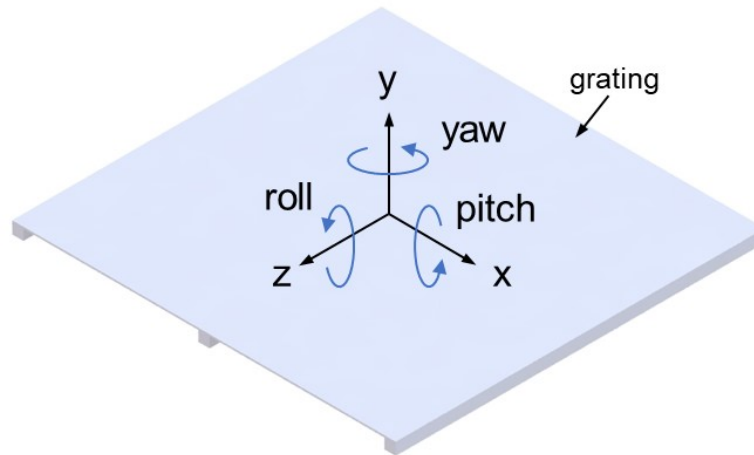
Figure 4: A single reflection grating in the OGRE spectrometer.[9] Each grating has three 2 mm wide ribs manufactured into the back of the substrate which allow light to pass through the grating stack while still maintaining the precisely manufactured wedge profile. Overlayed on this figure are the degrees of freedom for each reflection grating. The grooves for each grating converge in the $-\hat{z}$ direction to the spectrometer focal plane.

2.2.3 Grating-Level Alignment

With the grating pattern manufactured, the construction of an OGRE grating module can begin. Individual OGRE gratings start as wedged silicon substrates. These substrates are manufactured such that their wedge angle replicates the fan angle between neighboring gratings in each stack as required by the OGRE optical design. Each substrate will then be imprinted with the OGRE grating pattern ($\sim$ 70 mm x 70 mm) via substrate conformal imprint lithography.[10] The grating pattern will then be precisely diced from the wedged substrate such that the sides of each grating are aligned relative to the grating pattern itself. In addition to the dicing process, the majority of the backside of each grating substrate will be removed leaving a face sheet with a thickness of $\sim 0.3 - 0.5$ mm and three 2 mm wide x 70 mm long "ribs" (depicted in Figure 4). These ribs allow for light to still pass through each grating, but for the precise wedge profile to be maintained. The backside of each grating substrate is then etched to remove the stress introduced during this "ribbing" process. This completes the manufacture of a grating substrate.

Once individual grating substrates have been manufactured, they are then stacked on top of each other to realize aligned grating stacks. The wedged grating substrates themselves largely constrain the grating-level pitch, roll, and $\hat{y}$ alignment during this stacking process (degrees of freedom shown in Figure 4). A precision robot will be used to achieve alignment in the remaining three degrees of freedom ($\hat{x}$, $\hat{z}$, and yaw) by referencing the sides of each grating substrate. This alignment methodology is similar to that utilized for the silicon pore optic (SPO) technology developed by cosine Research B.V[11] – a collaborator on these alignment efforts.

The optical design of the spectrometer gives the desired placement of these gratings within the two stacks. However, the manufacture of each grating and the assembly of the 60 gratings into the two grating stacks will impart errors in the placement of each grating relative to their designed placement. These misalignments introduce aberrations into the observed LSF which will affect the achievable performance of the OGRE spectrometer. The impact of a grating-level misalignment in each degree of freedom is discussed below.

$\hat{x}$: The grating substrate will be diced from the grating substrate to an accuracy of $<$ 2 µm over the 70 mm length of the grating pattern. The stacking robot will then grab the diced substrate and place it in the stack. The precision of the stacking robot is $\lesssim$ 30 µm, but the interface between the robot and the grating substrate is currently unknown. In addition to the stacking robot itself, this interface is another source of error in the stacking process. Because this interface is currently unknown, the alignment tolerance in this degree of freedom has been set to $\pm$127 µm (3σ; standard machine tolerance). A misalignment at this level

Downloaded From: https://www.spiedigitallibrary.org/conference-proceedings-of-spie on 11 Feb 2021
Terms of Use: https://www.spiedigitallibrary.org/terms-of-use

mainly impacts the cross-dispersion extent of the observed LSF with an contribution of 102.6 µm HPD, but has a small effect on the dispersion direction as well (0.4 µm FWHM).

ŷ: The alignment in this degree of freedom is largely constrained by wedge manufacture. The manufacturer can easily meet standard machine tolerances in this degree of freedom, so this tolerance has been adopted in this degree of freedom: ± 127 µm (3σ). A ŷ misalignment at this level only has a slight contribution to the LSF extent in the dispersion direction: 0.8 µm FWHM.

ẑ: Just as with x̂ alignment, alignment in this degree of freedom is constrained largely by the stacking robot. Since the exact interface between the robot and the grating substrate is unknown, this tolerance has been set to ± 127 µm (3σ; standard machine tolerance). A ẑ misalignment at this level does not affect the observed LSF in the cross-dispersion direction, but has a significant impact on the dispersion direction: 8.5 µm FWHM.

Pitch (rotation about x̂): A pitch misalignment of the individual gratings relative to their nominal orientation acts to move the diffraction arc of each grating in the cross-dispersion direction. This will then increase the extent of the combined LSF in this dimension. The wedge manufacturer can achieve a tolerance on the wedge angle of ± 30 arcsec (3σ), so this tolerance has been adopted as the grating-level pitch alignment tolerance. A pitch misalignment of each grating at this level increases the extent of the LSF in the cross-dispersion direction by 489.9 µm HPD.

Yaw (rotation about ŷ): A yaw misalignment of the gratings within the grating stacks will increase the extent of the LSF in the cross-dispersion direction. The dicing process has an accuracy of < 2 µm over the 70 mm length of the grating such that the grating edges will be aligned to < 6 arcsec relative to the grating pattern itself. To limit the cross-dispersion impact on the LSF, the yaw alignment tolerance is ± 30 arcsec (3σ). A yaw misalignment at this level will increase the extent of the LSF in the cross-dispersion direction by 282.2 µm HPD and will slightly increase the extent in the dispersion direction by 0.6 µm FWHM.

Roll (rotation about ẑ): This degree of freedom is constrained both by wedge manufacture and the dicing process. The wedges can be manufactured such that the top and bottom surfaces are misaligned in roll by no more that ± 15 arcsec. The grating pattern will then be aligned to the wedge direction to within $\pm 0.5°$. Once aligned, the grating pattern is then diced to within < 2 µm over the 70 mm length of the grating. With the grating pattern aligned to within $\sim 0.5°$ of the wedge direction, there is no additional roll induced by a misalignment of the wedged substrate and the grating pattern. Therefore, the roll alignment tolerance is set to that which is achievable during wedge manufacture: ± 15 arcsec (3σ). A misalignment at this level increases the extent of the LSF in the dispersion direction by 10.8 µm FWHM and slightly increases the extent in the cross-dispersion direction by 5.7 µm HPD.

As mentioned previously, the interface between the stacking robot and the grating substrates is currently unknown. Therefore, there are some uncertainties in the achievable alignment of the gratings within stacks. While x̂ and ẑ alignment tolerances were purposefully set to standard machine tolerances to account for this unknown interface, the yaw tolerance is much tighter than can be achieved by standard machine tolerances. Further investigation will be needed to determine the interface between the grating substrates and the stacking robot, and if an additional constraint mechanism is needed. Precision pins are currently being investigated to serve as this additional constraint. Since the edges of the gratings will be aligned to < 6 arcsec relative to the grating pattern itself from the dicing process, each grating side can reference two precision pins to constrain grating yaw within a stack. Additionally, while the error budget baselines the wedged grating alignment methodology presented here and in Donovan et al. (2019), this error budget could easily be adapted for other grating alignment methods if needed.

2.2.4 Stack-Level Alignment

Once the grating stacks have been constructed, they must be aligned into the OGRE spectrometer. Rather than directly aligning the two stacks relative to the optic, the stacks will first be integrated into a grating module. This
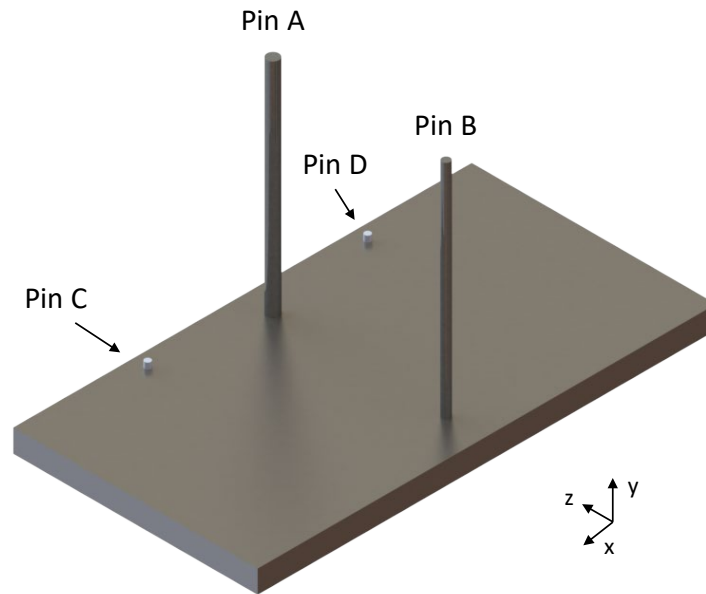
Figure 5: The anticipated alignment methodology for the two grating stacks to form a single grating module.[9] The two stacks would be placed on the bottom surface, then abutted against Pins A & B and either Pin C or Pin D. The precisely machined bottom plate constrains the $\hat{y}$, pitch, and roll of the grating stacks, while pins constrain the remaining three degrees of freedom – $\hat{x}$, $\hat{z}$, and yaw. Here, Pins A & B constrain the $\hat{x}$ and yaw alignment and Pins C & D constrain the $\hat{z}$ alignment between grating stacks.

eases spectrometer integration, but allows for additional misalignments to be introduced into the spectrometer and therefore additional aberrations to be introduced into the observed LSF.

Just as with grating-level alignment, the two stacks must be aligned in all six degrees of freedom. The currently envisioned stack-level alignment methodology utilizes a precisely polished surface and additional constraint pins to align the two stacks relative to one another. This system is depicted in Figure 5. The polished surface (polished to within ± 1 μm) orients the two stacks with respect to one another in $\hat{y}$, pitch, and roll, while the pins constrain the stacks in the three remaining degrees of freedom. The sides of grating stacks will be abutted against Pins A & B to constrain the two stacks in $\hat{x}$ and yaw, and the back of each grating stack will be abutted against either Pin C or Pin D to constrain the two stacks in the $\hat{z}$ direction. Further discussion of this alignment method can be found in O'Meara et al. (2019).[9] Each degree of freedom for stack-level alignment (as defined in Figure 5) and their impact on the LSF is discussed below.

$\hat{x}$: A misalignment in this degree of freedom acts to separate the LSFs formed by each grating stack in the cross-dispersion direction. Additionally, it has a small impact on the width of the LSF in the dispersion direction. Due to a weak dependence on both the dispersion and cross-dispersion extent, the $\hat{x}$ alignment tolerance has been set to the standard machine tolerance: ± 127 micron (3σ). This allows the two pins that constrain the two stacks in $\hat{x}$ (Pin A & Pin B) to be placed using standard machining techniques. A misalignment of ± 127 micron (3σ) contributes a dispersion extent of 1.0 μm FWHM and a cross-dispersion extent of $\sim 50-180$ μm HPD with the exact impact depending on the specifics of the relative stack-to-stack misalignment.

$\hat{y}$: A misalignment in this degree of freedom will separate the LSFs from each stack in the cross-dispersion direction. Because the wedged substrates are manufactured with a $\hat{y}$ tolerance of ± 127 μm (3σ), the maximum misalignment between the two stacks is ± 254 μm (3σ). A small error will also be introduced from the grating module base itself. However, this error $(\pm 1$ μm$)$ is negligible compared to the ± 254 μm (3σ)

uncertainty from wedged substrate manufacture. Therefore, the alignment tolerance in this degree of freedom will be $\pm 254\,\mu\mathrm{m}\,(3\sigma)$. This $\hat{y}$ misalignment will increase the total extent of the LSF in the cross-dispersion direction by $\sim 430 - 552\,\mu\mathrm{m}$ HPD.

$\hat{z}$: A misalignment in this degree of freedom will change the dispersion between the two stacks slightly such that the LSFs from each grating stack are dispersed to slightly different locations in the dispersion direction. This will increase the total extent of the LSF in the dispersion direction. This alignment will be constrained by pins (Pins C & D in Figure 5). Therefore, to ensure that this constraint can be placed using standard machining, a standard machine tolerance has been adopted in this degree of freedom: $\pm 127\,\mu\mathrm{m}\,(3\sigma)$. A misalignment at this level will increase the extent of the LSF in the dispersion direction by $\sim 3.6 - 6.7\,\mu\mathrm{m}$ FWHM, while only slightly impacting the extent in the cross-dispersion direction.

Pitch (rotation about $\hat{x}$): A pitch of one grating stack relative to the other grating stack will cause their individual LSF centroids to separate in the cross-dispersion direction. This will increase the total extent of the LSF formed by the two grating stacks. The relative pitch between stacks is governed by both the bottom grating in each grating stack and the flatness of the polished base. With a pitch tolerance on each grating substrate of ± 30 arcsec (3σ), the maximum misalignment between grating stacks induced by the stacks themselves is ± 60 arcsec (3σ). O'Meara et al. (2019) show that the worst-case scenario misalignment induced by the base is ± 12.7 arcsec misalignment per grating stack which gives a total base-induced misalignment between the two grating stacks of 25.4 arcsec.[9] However, they argue that the scenario assumed for this analysis is highly improbable and the likely base-induced misalignment is far below this value. Thus, it is assumed in this error budget that the grating-induced stack misalignment dominates the stack-level pitch misalignment, so a alignment tolerance of ± 60 arcsec (3σ) has been adopted. A pitch misalignment at this level will cause a $\sim 1800 - 1910\,\mu\mathrm{m}$ HPD change in the cross-dispersion extent of the LSF.

Yaw (rotation about $\hat{y}$): A yaw misalignment between grating stacks will cause the two LSFs formed by the two grating stacks to separate in the cross-dispersion direction, thus causing the total extent of the LSF in the cross-dispersion direction to grow. To limit the extent of the LSF in the cross-dispersion direction, this alignment tolerance has been set to ± 60 arcsec (3σ). This leads to a $\sim 1020 - 1130\,\mu\mathrm{m}$ HPD growth in the cross-dispersion extent of the LSF. O'Meara et al. (2019) show that this alignment tolerance is achievable by abutting the two grating stacks against a set of precision pins (Pins A & B in Figure 5) machined via wire electrical discharge machining (wire EDM).[9]

Roll (rotation about $\hat{z}$): The misalignment of the two grating stacks in roll will cause the individual LSFs (which are much narrower in the dispersion direction when compared to the cross-dispersion direction) to tilt with respect to the mean dispersion direction of the two grating stacks. This will cause the combined LSF to have a greater extent in the dispersion direction. As with stack-level pitch, the stack-to-stack roll alignment is constrained by both the bottom grating in the grating stack and the polished base of the grating module. The grating substrates themselves have a roll requirement of ± 15 arcsec (3σ), which results in a maximum stack misalignment of ± 30 arcsec (3σ). Additionally, the base can contribute a misalignment of 12.6 arcsec per stack for a total base-induced roll misalignment of 25.2 arcsec as derived in O'Meara et al. (2019).[9] However, just as with stack-level pitch, this induced misalignment is highly improbable and will likely be much lower than this value. Thus, a ± 30 arcsec (3σ) has been adopted as the alignment tolerance in roll. This misalignment results in a LSF impact of $26.9 - 31.0\,\mu\mathrm{m}$ FWHM in the dispersion direction.

A summary of the derived stack-level tolerances can be seen in Table 2. For stack-to-stack alignment, pitch and yaw misalignments have the largest impact on the extent of the LSF in the cross-dispersion direction, while misalignments in $\hat{z}$ and roll have the largest impacts on the extent in the dispersion direction.

2.2.5 Grating-Module-To-Optic Alignment

With a grating module fully assembled, it then must be aligned to the optic. Compared to the induced errors from grating-level and stack-level misalignments, induced errors due to misalignments between the grating module

Table 3: Errors induced by a misalignment of the optical assembly (aligned OGRE mirror module + OGRE grating module) into the observed LSF of the OGRE spectrometer. Shown are the 3σ level (99.7%) requirements for each error in all six degrees of freedom (DoF) and the impact of the error in both the dispersion direction (measured as a full-width at half maximum [FWHM]) and the cross-dispersion direction (measured as a half-power diameter [HPD]).

		Requirements (3σ Level)				LSF Impact			
						Dispersion Direction		Cross-Disp. Direction	
Error	DoF	μm (±)		arcsec (±)		FWHM [μm]		HPD [μm]	
	X	-600	-600			0.0	0.0	0.0	0.0
	Y	-1000	1000			0.0	0.0	0.0	0.0
Optical Assembly To Nominal	Z	-500	500			13.5	14.8	0.0	0.0
Focal Plane	Pitch (X)			-60	60	0.0	0.0	0.0	0.0
	Yaw (Y)			-90	90	7.9	4.6	0.0	0.0
	Roll (Z)			-1000	1000	0.0	0.0	0.0	0.0
RSS Total						15.6	15.5	0.0	0.0

and the optic do not contribute as significantly to the observed LSF. Furthermore, the contributions due to grating-module-to-optic misalignments move the entire LSF on the focal plane, but do not affect its total extent in the dispersion and cross-dispersion directions. This allows alignment tolerances to be slightly looser when compared to grating-level and stack-level alignment tolerances as shown in Table 2.

Since grating-module-to-optic alignment does not impact the extent of the LSF to any large degree, the goal of assigning alignment tolerances for this error term is to keep the LSF on the detector. Misalignments in $\hat{x}$, $\hat{y}$, pitch, and yaw all shift the LSF centroid in the cross-dispersion direction. A movement of $< \pm 1$ mm in the cross-dispersion direction has been adopted as the maximum movement that the LSF centroid can be shifted for each of these misalignments. The size of the detector is $\sim 25 \times 25$ mm^2, so even if all four misalignments contributed maximally, the movement of the LSF centroid would be limited to ~ 4 mm. To limit the movement in this dimension to ± 1 mm, $\hat{x}$ and $\hat{y}$ misalignments have each been given a tolerance of ± 500 μm (3σ). They contribute insignificantly to the extent of the LSF in the dispersion and cross-dispersion directions. Similarly, pitch and yaw misalignments each have a tolerance of ± 60 arcsec (3σ) to limit their cross-dispersion movement to $< \pm 1$ mm. Pitch and yaw misalignments at this level both contribute insignificantly to the LSF extent.

A misalignment in roll contributes directly to a movement of the LSF centroid in the dispersion direction, since the dispersion direction will change with the roll of the grating module. The goal when assigning an alignment tolerance to this degree of freedom is to keep important lines in the soft X-ray spectrum of Capella on the detector. To satisfy this requirement, the roll tolerance of the grating module relative to the optic has been set to ± 120 arcsec (3σ).

The remaining misalignment to be considered is a $\hat{z}$ misalignment. At the millimeter level, this misalignment only changes the dispersion relation (Eq. 2) on the focal plane. A large change in dispersion on the focal plane will move important lines off the focal plane. A ~ 1 mm movement of the grating module relative to the optic does not have any appreciable change in the dispersion on the focal plane though. Therefore, the alignment tolerance for this degree of freedom is somewhat arbitrary. The $\hat{z}$ alignment tolerance has been set to ± 1 mm (3σ) – a value which should be easily achievable through standard machine tolerances (even with the stack-up of several interfaces manufactured to standard machine tolerances). A summary of these misalignments and their impact on the observed LSF can be seen in Table 2.

2.3 Optical Assembly Contributions

The aligned grating module and optic becomes the "optical assembly". This optical assembly must be aligned to the nominal focal plane. Whereas the grating-level, stack-level, and grating-module-to-optic alignment tolerances concern components within close proximity to one another, the optical assembly is ~ 3.5 m away from the nominal focal plane. This introduces new challenges that must be considered when assigning alignment tolerances to this component. Each degree of freedom (as depicted in Figure 2) for this alignment is discussed below.

$\hat{x}$: A misalignment in this degree of freedom moves the optical assembly in the dispersion direction relative to the nominal focal plane. This in turn moves the observed LSF on the spectral detectors in the dispersion

direction. To keep important lines in the soft X-ray spectrum of Capella on the detector, the $\hat{x}$ alignment tolerance has been set to ± 600 µm (3σ).

$\hat{y}$: A misalignment here causes the optical assembly to move in the cross-dispersion direction relative to the nominal focal plane. This then causes the observed LSF to move in the cross-dispersion direction on the spectral detectors. Similar to other LSF centroid translational errors, an alignment tolerance is chosen to limit the movement of the observed LSF on the focal plane to $< \pm 1$ mm. This equates to an alignment tolerance of ± 1000 µm (3σ).

$\hat{z}$: A shift in the optical assembly relative to the nominal focal plane in this dimension moves the observed LSF from its nominal focus position. A misalignment here then acts to defocus the spectrometer which contributes to the LSF extent in the dispersion direction. To limit the impact on the extent of the LSF in the dispersion direction, while taking into consideration the practicality of aligning two components over a ~ 3.5 m distance, this alignment tolerance has been set to ± 500 µm (3σ). A misalignment at this level increases the LSF extent in the dispersion direction by $13.5 - 14.8$ µm FWHM.

Pitch (rotation about $\hat{x}$): A pitch of the optical assembly relative to the nominal focal plane acts to move the LSF in the cross-dispersion direction. Similar to other LSF centroid translational errors, the translation was limited to $< \pm 1$ mm, which corresponds to an alignment tolerance of ± 60 arcsec (3σ).

Yaw (rotation about $\hat{y}$): Similar to a yaw misalignment between the grating module and the optic, a yaw misalignment of the optical assembly relative to the nominal focal plane will move the centroid of the observed LSF in the cross-dispersion direction. This movement was limited to $< \pm 1$ mm (3σ), which corresponds to an alignment tolerance of ± 90 arcsec. This has a slight impact on the extent of the LSF in the dispersion direction as well ($\sim 4.6 - 7.9$ µm FWHM).

Roll (rotation about $\hat{z}$): A roll misalignment of the optical assembly relative to the nominal focal plane moves the observed LSF in the dispersion direction. To keep important spectral lines on the detector, this tolerance has been set to $\pm 0.28°$ ($= \pm 1000$ arcsec).

The optical assembly will be mounted onto an optical bench cantilevered off of a mounting point close to the focal plane of the spectrometer. To achieve the derived alignment tolerances (as summarized in Table 3), a kinematic mount will be designed as an interface between the optical assembly and the optical bench. This mount would provide movement $\hat{z}$, pitch, and yaw – the degrees of freedom with the tightest alignment tolerances.

A concern with the alignment of the optical assembly is maintaining this alignment during flight. Typically, this optical bench is made from several cylindrical aluminum sections. However, it is anticipated that this aluminum optical bench cannot maintain the derived alignment tolerances due to potential thermal gradients over the length of the bench which would cause an expansion/contraction of the optical bench. To better constrain the optical assembly orientation relative to the nominal focal plane, a custom rigid optical bench will be developed. Past suborbital rocket payloads have used optical benches made from carbon fiber.[12]

2.4 Detector Contributions

The last static component of the OGRE spectrometer to consider is the alignment of the spectral detectors relative to the nominal spectrometer focal plane. Just as with all other potential misalignments, this component can be misaligned in all six degrees of freedom. A discussion of each degree of freedom and the impact of a misalignment in each of these degrees of freedom (as depicted in Figure 2) is discussed below.

$\hat{x}$: A misalignment in this degree of freedom causes a shift of the detector in the dispersion direction relative to the nominal focal plane. If shifted too far, important spectral lines from Capella will begin to fall off of the detector. To keep important lines on the detector, an alignment tolerance of ± 600 µm has been assigned to this degree of freedom.

Table 4: Errors induced in the observed LSF of the OGRE spectrometer by a misalignment of a spectral detector relative to the nominal focal plane . Shown are the 3σ level (99.7%) requirements for each error in all six degrees of freedom (DoF) and the impact of the error in both the dispersion direction (measured as a full-width at half maximum [FWHM]) and the cross-dispersion direction (measured as a half-power diameter [HPD]).

| | | Requirements (3σ Level) | | | | LSF Impact | | | |
| | | | | | | Dispersion Direction | | Cross-Disp. Direction | |
Error	DoF	μm (±)		arcsec (±)		FWHM [μm]		HPD [μm]	
Detector To Nominal Focal Plane	X	-600	600			0.0	0.0	0.0	0.0
	Y	-254	254			0.0	0.0	0.0	0.0
	Z	-254	254			7.2	8.0	0.0	0.0
	Pitch (X)			-3600	3600	0.0	0.0	0.0	0.0
	Yaw (Y)			-3600	3600	0.0	0.0	0.0	0.0
	Roll (Z)			-3600	3600	0.0	0.0	0.0	0.0
RSS Total						7.2	8.0	0.0	0.0

ŷ: A misalignment here causes the detector to move in the cross-dispersion direction relative to the nominal focal plane. As a result of this movement, the observed LSF will move on the detector. However, the observed LSF just needs to remain on the detector. An alignment tolerance of ±254 µm has been assigned here, but realistically this could be loosened if necessary.

ẑ: A shift in $\hat{z}$ of the detector relative to the nominal focal plane moves the observed LSF away from its nominal focus position. A misalignment here then acts to defocus the spectrometer which introduces aberrations into the LSF in the dispersion direction. To limit the impact on the extent of the observed LSF in the dispersion direction, this alignment tolerance has been set to ±254 µm. A misalignment at this level increases the LSF extent in the dispersion direction by $7.2 - 8.0$ µm FWHM.

Pitch (rotation about $\hat{x}$): A pitch of the detector (about its center) relative to the nominal focal plane will act to defocus the LSF – one half of the LSF will be intrafocal and the other half will be extrafocal. However, only relatively large pitches ($> 2°$) will cause any appreciable impact on the extent of the observed LSF. Therefore, a relatively loose tolerance of $±1°= 3600$ arcsec has been adopted here. This tolerance can be loosened if necessary.

Yaw (rotation about $\hat{y}$): Similar to a misalignment of the detector in pitch, a yaw misalignment of the detector (about its center) relative to the nominal focal plane will move the portions of the spectrum on the detector out of its nominal focal position. Again though, only large yaws ($> 2°$) will lead to any appreciable impact on the observed LSF. Therefore, the same $±1°= 3600$ arcsec alignment tolerance has been adopted here, but this could be loosened if necessary.

Roll (rotation about $\hat{z}$): A roll of the detector relative to the nominal focal plane will have no impact on the observed LSF. Its alignment tolerance has been set to $±1°= 3600$ arcsec, but this is somewhat arbitrary.

As shown in Table 4, detector contributions only impact the extent of the observed LSF at the $\sim 7 - 8$ µm level. Compared to contributions from the grating and the optic, the detector does not impact the LSF to any appreciable degree.

One complication in the alignment of the detectors is that their placement within their packaging from the manufacturer (e2v) is not known to the level of the derived alignment tolerances. Therefore, their placement must be reconstructed once assembled and then adjusted to move them into their optimal location within the alignment tolerances. Since the detectors cannot be touched by traditional measuring devices such as a portable measuring arm, a non-contact measuring method is required. The baseline method for this non-contact measurement is a laser scanner attachment to a portable measuring arm. With an accuracy of ~ 40 µm, this laser scanner would easily be able to measure each detector within its packaging to the required accuracy. With its position and orientation known with respect to its packaging, each detector could then be adjusted to place it within its alignment tolerances.

Table 5: All errors contributing to the observed LSF of the OGRE spectrometer, including errors from the optic module, grating module, optical assembly (aligned optic + grating module), detector, and in-flight contributions. Listed is each error and its contribution to the observed LSF in both the dispersion direction (measured as a full-width at half maximum [FWHM]) and the cross-dispersion direction (measured as a half-power diameter [HPD]).

	LSF Impact			
	Dispersion Direction		**Cross-Disp. Direction**	
Component	**FWHM [µm]**		**HPD [µm]**	
Optic	25.4		84.8	
Grating	40.8	38.0	2316.2	2251.2
Optic Assembly	15.6	15.5	0.0	0.0
Detector	7.2	8.0	0.0	0.0
RSS - Static Contributions	51.0	48.9	2317.7	2252.8
Jitter	17.0		14.4	
RSS - Dynamic Contributions	17.0		14.4	
RSS - Static + Dynamic	53.8	51.8	2317.8	2252.9

2.5 In-Flight Contributions: Jitter

The final contributor to the LSF of the OGRE spectrometer is the in-flight contribution from jitter – the pointing stability of the payload during flight. This movement of the payload about the source will artificially increase the size of the source, and therefore impacts the extent of the observed LSF in both the dispersion and cross-dispersion directions.

The NASA Sounding Rockets User Handbook[13] states that the NSROC (NASA Sounding Rocket Operations Contract) Celestial Attitude Control System can achieve a jitter of < 1 arcsec/sec FWHM in its linear thrust configuration (the configuration baselined for the OGRE mission). This number has also been confirmed from past sounding rocket flight data. Therefore, this number is adopted as the jitter requirement for the OGRE spectrometer: < 1 arcsec/sec FWHM. This requirement corresponds to an induced aberration of 17 µm FWHM in the dispersion direction and 14.4 µm HPD in the cross-dispersion direction of the LSF.

3. COMBINING LSF ERRORS

With all performance requirements and alignment tolerances derived, they can be combined to inform the achievable performance of the OGRE spectrometer. The question then becomes how do these individual errors combine? Are they all independent and therefore add in quadrature, or do they combine in a less straightforward manner? To explore each of these possibilities, the errors were first analyzed as if they were independent. Then, a raytrace simulation of the OGRE spectrometer with these same errors and misalignments was performed to compare the results.

3.1 The RSS Method: Independent Errors

If each induced error to the LSF is asssumed to be independent with respect to other induced errors, the LSF errors add in quadrature (root sum of the squares; RSS). In Tables 1-4, the individual errors from each component were added in quadrature with their total LSF impact ("RSS Total") displayed at the bottom of each table. Each of these totals was collected and is displayed in Table 5. The totals from each component were then added in quadrature to yield a total LSF impact in both the dispersion and cross-dispersion directions. The resulting total impact on the observed LSF is $\sim 51.8 - 53.8$ µm FWHM in the dispersion direction and $\sim 2250 - 2320$ µm HPD in the cross-dispersion direction. Converting the extent of the LSF in the dispersion direction (Δx) to spectral resolution ($R = x/\Delta x$ with $x = 98.2$ mm), the maximum achievable spectral resolution if all LSF errors added in quadrature is $R \approx 1830 - 1900$. This result is slightly below the spectral resolution goal of $R > 2000$,
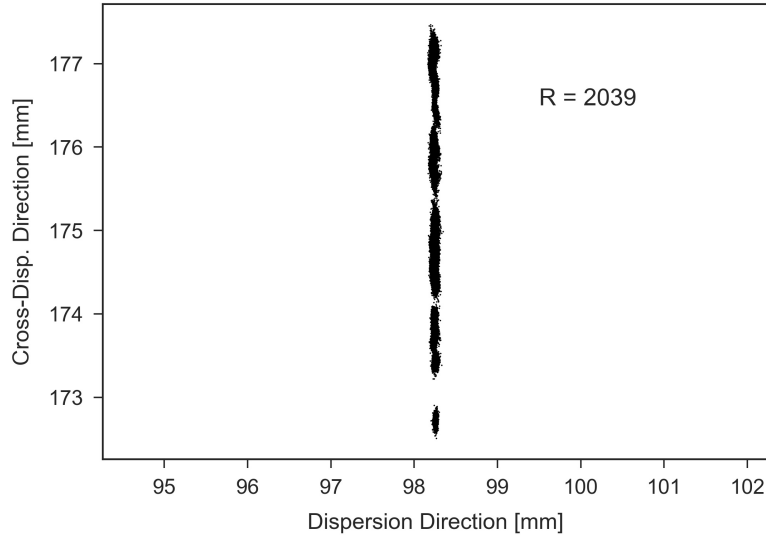
Figure 6: Results from a raytrace simulation of the OGRE spectrometer with misalignments and performance errors at their 3σ tolerances and requirements. In this simulation, the spectrometer achieved a resolution of $R = 2039$ at $n\lambda = 4.76$ nm – the central wavelength on the spectral detectors. This performance is larger than the performance predicted if one assumed that each error was independent and thus added in quadrature.

but it still comfortably meets the resolution requirement of $R > 1500$. However, is it correct to assume that all of these errors are independent and add in quadrature?

3.2 Raytrace Simulation Results

To test whether or not it is correct to assume that all error are independent and add in quadrature, a raytrace simulation of the OGRE spectrometer was performed with the derived performance requirements, alignment tolerances, and jitter requirement at the wavelength that diffracts to the center of the spectral detectors in the OGRE spectrometer: $n\lambda = 4.76$ nm. All misalignments and performance errors were assumed to be at their maximum value (the 3σ limit). The results of the raytrace simulation are shown in Figure 6. As can be seen in this figure, the achievable spectral resolution here is slightly higher: $R \approx 2040$. This is slightly above the spectral resolution goal of $R > 2000$.

4. FUTURE WORK

The results of the raytrace simulation indicate that the errors presented herein do not add in quadrature and that they therefore are not independent. However, this result was from a single raytrace simulation. Further analysis and raytrace simulations are needed to verify these results. For example, the raytrace simulation was performed with all performance errors and misalignments contributing at their 3σ limit. However, these errors and misalignments will not actually all contribute at this level simultaneously. Additionally, there could be variations between each raytrace simulation that affect the simulated performance of the spectrometer. Further simulations will need to be performed to better inform the performance of the spectrometer.

Furthermore, the alignment processes for all components in the OGRE spectrometer are continually under development. While the idealized processes acted as inputs to the presented error budget, there will be adjustments that will need to be made as these alignment activities begin. For example, some tolerances that were expected to be easily achievable might not be as easily achievable as once envisioned and vice versa. To account for this eventuality, the error budget was designed such that individual misalignments and/or errors can be adjusted and their impact on the LSF will be updated in real time. This allows the user to experiment with relative LSF impacts from different misalignments and/or errors. Thus, if these errors or alignment tolerances need to be

adjusted for the spectrometer, the error budget is equipped to inform how the performance requirements and/or goals of the OGRE spectrometer can be recovered.

5. SUMMARY

In this manuscript, a comprehensive LSF error budget for the soft X-ray grating spectrometer on the Off-plane Grating Rocket Experiment (OGRE) was described. This error budget described potential impacts to the LSF observed by the OGRE spectrometer including component misalignments and performance errors, derived realistic alignment tolerances for component misalignments, and elucidated how each misalignment and performance error impacted the observed LSF. The impacts from component misalignments and performance errors were combined first by assuming independent errors such that the errors added in quadrature. The same misalignments and performance errors were then simulated via a raytrace simulation. The results indicate that the OGRE spectrometer should be able to comfortably meet its spectral resolution requirement and even its goal at select energies.

ACKNOWLEDGMENTS

REFERENCES

[1] Donovan, Benjamin D. McEntaffer, R. L., Tutt, J. H., O'Meara, B. C., Grisé, F., Allgood, K. D., Biskach, M. P., Chan, K.-W., Hlinka, M., Kearney, J. D., Mazzarella, J. R., McClelland, R. S., Numata, A., Riveros, R. E., Saha, T. T., Solly, P. M., Zhang, W. W., Holland, A. D., Lewis, M. R., Soman, M. R., and Holland, K., "An Updated Optical Design for the Off-plane Grating Rocket Experiment," (these proceedings).

[2] Zhang, W. W., Allgood, K. D., Biskach, M. P., Chan, K.-W., Hlinka, M., Kearney, J. D., Mazzarella, J. R., McClelland, R. S., Numata, A., Riveros, R. E., Saha, T. T., and Solly, P. M., "Astronomical x-ray optics using mono-crystalline silicon: high resolution, light weight, and low cost," *Proc. SPIE* **10699**, 106990O (2018).

[3] McEntaffer, R., DeRoo, C., Schultz, T., Gantner, B., Tutt, J., Holland, A., O'Dell, S., Gaskin, J., Kolodziejczak, J., Zhang, W. W., Chan, K., Biskach, M., McClelland, R., Iazikov, D., Wang, X., and Koecher, L., "First results from a next-generation off-plane X-ray diffraction grating," *Experimental Astronomy* **36**, 389–405 (Aug 2013).

[4] Lewis, M. R. F., Soman, M. R., Holland, A. D., Murray, N. J., Hall, D., Weatherill, D. P., Tutt, J. H., McEntaffer, R. L., DeRoo, C. T., Schultz, T. B., and Holland, K., "Development of the x-ray camera for the OGRE sub-orbital rocket," *Proc. SPIE* **9915**, 991506 (2016).

[5] Miles, D. M., McCoy, J. A., McEntaffer, R. L., Eichfeld, C. M., Lavallee, G., Labella, M., Drawl, W., Liu, B., DeRoo, C. T., and Steiner, T., "Fabrication and Diffraction Efficiency of a Large-format, Replicated X-Ray Reflection Grating," *ApJ* **869**(2), 95 (2018).

[6] Cash, W. C., "X-ray spectrographs using radial groove gratings," *Appl. Opt.* **22**, 3971–3976 (Dec 1983).

[7] Zhang, W. W., Allgood, K. D., Biskach, M. P., Chan, K.-W., Hlinka, M., Kearney, J. D., Mazzarella, J. R., McClelland, R. S., Numata, A., Riveros, R. E., Saha, T. T., and Solly, P. M., "High-resolution, lightweight, and low-cost x-ray optics for the Lynx observatory," *Journal of Astronomical Telescopes, Instruments, and Systems* **5**, 021012 (2019).

[8] Donovan, B. D., "Performance Testing of X-Ray Reflection Gratings Produced via Electron-Beam Lithography," *Applied Optics* (In Prep).

[9] O'Meara, B. C., Donovan, B. D., Tutt, James H.and McEntaffer, R. L., Schultz, T. B., Allgood, K. D., Biskach, M. P., Chan, K.-W., Hlinka, M., Kearney, J. D., Mazzarella, J. R., McClelland, R. S., Numata, A., Riveros, R. E., Saha, T. T., Solly, P. M., Zhang, W. W., Holland, A. D., Lewis, M. R., Soman, M. R., and Holland, K., "The opto-mechanical design for the Off-plane Grating Rocket Experiment," (these proceedings).

[10] Verschuuren, M. A., Megens, M., Ni, Y., van Sprang, H., and Polman, A., "Large area nanoimprint by substrate conformal imprint lithography (SCIL)," *Advanced Optical Technologies* **6**, 243–264 (2017).

[11] Collon, M. J., Vacanti, G., Barriere, N., Landgraf, B., Guenther, R., Vervest, M., van der Hoeven, R., Chatbi, A., Girou, D., Sforzini, J., Beijersbergen, M. W., Bavdaz, M., Wille, E., Fransen, S., Shortt, B., Haneveld, J., Booysen, K., Koelewijn, A., Wijnperlé, M., van Baren, C., Eigenraam, A. e., Müller, P., Krumrey, M., Burwitz, V., Spiga, D., Pareschi, G., Massahi, S., Christensen, F., Della Monica Ferreira, D., Valsecchi, G., Oliver, P., Chequer, I., Ball, K., and Zuknik, K.-H., "Silicon pore optics mirror module production and testing," *Proc. SPIE* **10699**, 106990Y (2018).

[12] France, K., Hoadley, K., Fleming, B. T., Kane, R., Nell, N., Beasley, M., and Green, J. C., "The SLICE, CHESS, and SISTINE Ultraviolet Spectrographs: Rocket-Borne Instrumentation Supporting Future Astrophysics Missions," *Journal of Astronomical Instrumentation* **5**, 1640001 (Dec 2016).

[13] NASA Goddard Space Flight Center - Sounding Rockets Program Office, "NASA Sounding Rockets User Handbook."